

PAPER

Excited quantum anomalous and spin Hall effect: dissociation of flat-bands-enabled excitonic insulator state

To cite this article: Yinong Zhou *et al* 2022 *Nanotechnology* **33** 415001

View the [article online](#) for updates and enhancements.

You may also like

- [Nonlinear compact localized modes in flux-dressed octagonal-diamond lattice](#)
M G Stojanovi, S Gündodu, D Leykam et al.
- [Properties of fibreboard \(FBs\) and recycle fibreboard \(rFBs\) and analysis of their wastage after recycling](#)
A Nuryawan, I Risnasari, A P Pohan et al.
- [IceCube Constraints on the Fermi Bubbles](#)
Nimrod Sherf, Uri Keshet and Ilya Gurwich



ECS Membership = Connection

ECS membership connects you to the electrochemical community:



- Facilitate your research and discovery through ECS meetings which convene scientists from around the world;
- Access professional support through your lifetime career;
- Open up mentorship opportunities across the stages of your career;
- Build relationships that nurture partnership, teamwork—and success!

Join ECS!

Visit electrochem.org/join



Excited quantum anomalous and spin Hall effect: dissociation of flat-bands-enabled excitonic insulator state

Yinong Zhou¹ , Gurjyot Sethi¹, Hang Liu^{2,3} , Zhengfei Wang⁴  and Feng Liu¹ 

¹Department of Materials Science and Engineering, University of Utah, Salt Lake City, UT 84112, United States of America

²Songshan Lake Materials Laboratory, Dongguan, Guangdong 523808, People's Republic of China

³Beijing National Laboratory for Condensed Matter Physics and Institute of Physics, Chinese Academy of Sciences, Beijing 100190, People's Republic of China

⁴Hefei National Laboratory for Physical Sciences at the Microscale, CAS Key Laboratory of Strongly-Coupled Quantum Matter Physics, University of Science and Technology of China, Hefei, Anhui 230026, People's Republic of China

E-mail: fliu@eng.utah.edu

Received 31 January 2022, revised 19 May 2022

Accepted for publication 20 June 2022

Published 19 July 2022



CrossMark

Abstract

Quantum anomalous Hall effect (QAHE) and quantum spin Hall effect (QSHE) are two interesting physical manifestations of 2D materials that have an intrinsic nontrivial band topology. In principle, they are ground-state equilibrium properties characterized by Fermi level lying in a topological gap, below which all the occupied bands are summed to a non-zero topological invariant. Here, we propose theoretical concepts and models of 'excited' QAHE (EQAHE) and EQSHE generated by dissociation of an excitonic insulator (EI) state with complete population inversion (CPI), a unique *many-body* ground state enabled by two yin-yang flat bands (FBs) of opposite chirality hosted in a diatomic Kagome lattice. The two FBs have a trivial gap in between, i.e. the system is a trivial insulator in the *single-particle* ground-state, but nontrivial gaps above and below, so that upon photoexcitation the quasi-Fermi levels of both electrons and holes will lie in a nontrivial gap achieved by the CPI-EI state, as demonstrated by exact diagonalization calculations. Then dissociation of singlet and triplet EI state will lead to EQAHE and EQSHE, respectively. Realizations of yin-yang FBs in real materials are also discussed.

Supplementary material for this article is available [online](#)

Keywords: flat band, quantum anomalous Hall effect, quantum spin Hall effect, excitonic insulator state, complete population inversion, diatomic Kagome lattice

(Some figures may appear in colour only in the online journal)

Quantum Hall effect (QHE) displays a quantized Hall conductivity that is only determined by physical constants [1] and fundamentally rooted in topological electronic states [2–5]. It was observed in a 2D electron gas subjected to a strong magnetic field [1] that splits the parabolic electronic bands into discrete Landau levels (LLs), each characterized with a Chern number $C = 1$ [2–5]. For QHE, the quantized

transverse Hall conductivity equals the filling of LLs (n), $\sigma_{xy} = n \cdot e^2/h$ (figure 1(a)), where n can be either an integer or a specific fractional number. Haldane proposed a condensed-matter version of QHE without LLs [the quantum anomalous Hall effect (QAHE)] in a Chern insulator, featured with a topological gap separating the valence bands (VBs) having a non-zero Chern number (e.g. $C = 1$) from the conduction

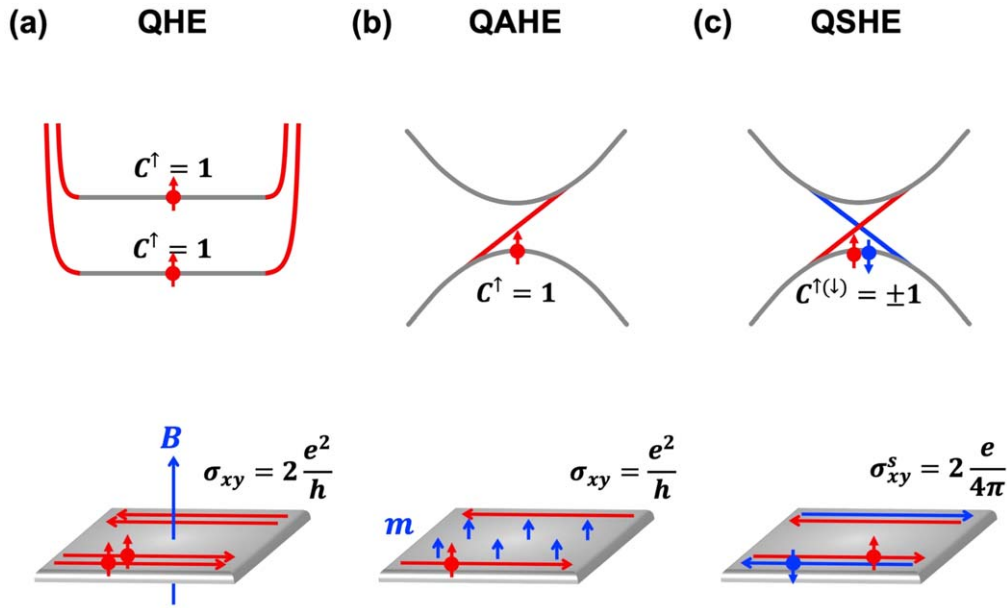


Figure 1. Schematic illustration comparing three types of quantized charge and spin Hall effects. The upper panel shows the electronic states associated with each effect: (a) QHE featured with LLs and a chiral edge state (red). Each LL carries a Chern number $C = 1$. (b) QAHE, a Chern insulator state, featured with a topological gap between a dispersive VB of $C = 1$ and a dispersive CB of $C = 0$, and a chiral edge state in the gap (red). (c) QSHE, a topological insulator state, featured with a topological gap between a dispersive VB of spin Chern number $C^s = 1/2(C^\uparrow - C^\downarrow) = 1$ and a dispersive CB of $C^s = 0$, a pair of helical edge states in the gap (red and blue lines). The lower panel illustrates the quantized charge or spin Hall conductivity carried by topological edge states: (a) $\sigma_{xy} = 2 \cdot e^2/h$ with two filled LLs (see upper panel). (b) $\sigma_{xy} = e^2/h$ for a Chern insulator with $C = 1$. (c) $\sigma_{xy}^s = 2 \cdot e/4\pi$ for a topological insulator with $C^s = 1$. Note that in (b,c), only bands of interest around Fermi level with their non-zero Chern number are labeled. If all VBs and CBs are present, the sum of their Chern numbers must equal zero.

bands (CBs). It gives rise to a $\sigma_{xy} = C \cdot e^2/h$ (figure 1(b)). Recently, the quantum spin Hall effect (QSHE) was theoretically proposed by Kane-Mele [6] and Bernevig-Hughes-Zhang [7], featured with a topological gap separating the VBs having a non-zero Z_2 [8] or sum of spin Chern number of each VB [9] (e.g. $C^s = 1$) from the CBs. It gives rise to a spin Hall conductivity $\sigma_{xy}^s = C^s \cdot e/2\pi$ (figure 1(c)). Both QAHE [10] and QSHE [11] have been experimentally confirmed in real materials. These pioneering works have fostered an ever-growing field of topological physics and materials.

QHE, QAHE, and QSHE are all intrinsically *single-particle* ground-state properties characterized with the Fermi level lying in a topological gap. Now, let us imagine a band structure that contains two enantiomorphic (yin-yang) flat bands (FBs) of opposite chirality, i.e. opposite Chern numbers, featured with one trivial gap in between and two topological gaps above and below, as shown in figure 2(a). At the ground state, the system is a semiconductor or normal insulator characterized with the Fermi level lying in a trivial gap between the two FBs. Upon photoexcitation, the quasi-Fermi levels of electrons and holes will lie in the topological gap above the top FB and below the bottom FB (figures 2(b), (c)), respectively, when complete population inversion (CPI) between the two FBs is achieved in the EI state, a *many-body* ground state [12]. Consequently, dissociation of a singlet or triplet EI state will lead to “excited” quantum anomalous Hall effect (EQAHE) or quantum spin Hall effect (EQSHE), as the former breaks while the latter preserves the time-reversal symmetry (TRS).

Then, a ribbon structure possesses the above-mentioned band structure with open edges. The system is originally insulated with a gap separating a fully occupied valence FB and empty conduction FB. Suppose a left-handed circularly polarized light (σ^+ -CPL) excites spin-up electrons into the conduction FB, leaving behind spin-down holes in the valence FB, forming a singlet excitonic state [13, 14]. Usually, the excitons, such as for non-equilibrium valley Hall effect, have a positive formation energy, i.e. a binding energy smaller than the band gap, which are unstable as an excited state. However, in the EI state, the excitons have a negative formation energy, which are stable with infinite lifetime as a many-body ground state. Consequently, if CPI between two FBs can be achieved, then the quasi-Fermi level of electrons (holes) in the conduction (valence) band lies in the topological gap with edge states at equilibrium (figure 2(b) upper panel). Under an external bias, the dissociated spin-up electrons conduct via the chiral edge state within the topological gap between the conduction FB and the dispersive band above (see solid red line in figure 2(b)), and spin-down holes conduct via the chiral edge state within the topological gap between the valence FB and the dispersive band below (see dashed blue line in figure 2(b)). The spin-up electrons and the spin-down holes propagate in the opposite directions along the two opposite edges of a ribbon sample (see figure 2(b) lower panel), enabling a quantized conductance $\sigma_{xy} = -e^2/h$, while the bulk is still insulating. The total charge Hall conductivity is $\sigma_{xy} = -2 \cdot e^2/h$ (figure 2(b) lower panel). The reverse is true for the right-handed CPL.

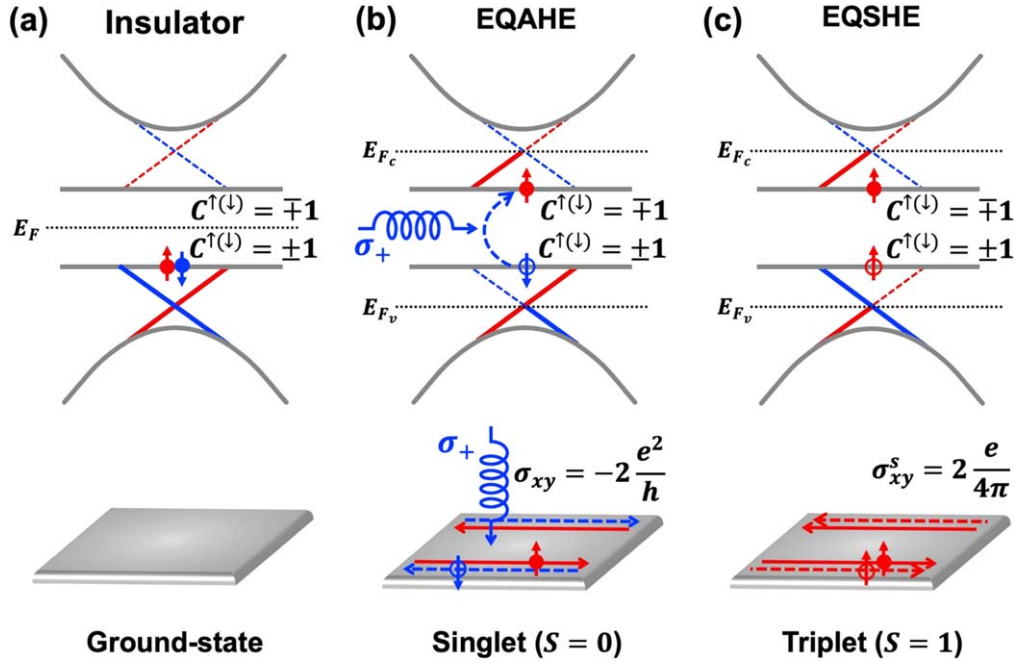


Figure 2. Schematic illustration of the excited quantum anomalous Hall effect (EQAHE) and quantum spin Hall effect (EQSHE). The upper panel shows the electronic states associated with each effect: (a) ground-state of the system with yin-yang FBs. (b) Singlet excitonic state with a spin-up electron in the conduction FB and a spin-down hole in the valence FB induced by a σ^+ -CPL. (c) Triplet excitonic state with a spin-up electron in the conduction FB and a spin-up hole in the valence FB. The quasi-Fermi level of electrons (holes) in the conduction (valence) band is labeled as E_{F_c} (E_{F_v}). The red/blue solid/dashed lines indicate the population of the edge states. The lower panel illustrates the quantized charge or spin Hall conductivity carried by topological edge states: (a) no edge states for the intrinsic semiconductor. (b) $\sigma_{xy} = -2 \cdot e^2/h$ for EQAHE with an opposite-spin electron–hole pair created in yin-yang FBs of the opposite Chern number. (c) $\sigma_{xy}^s = 2 \cdot e/4\pi$ for EQSHE with a same-spin electron–hole pair created in yin-yang FBs of the same Chern number.

Effectively the yin-yang FBs behave like a condensed-matter version of two LLs, albeit with an electron and a hole occupying two LLs with opposite Chern numbers, respectively. It can be viewed as a pair of electron- and hole-conducting QAHE or two copies of half QSHE. A more detailed illustration of the EQAHE is available in figure S1, in comparison with valley Hall effect [15–19]. See also supplementary material for other details [20–26], available online at stacks.iop.org/NANO/33/415001/mmedia.

For the triplet excitonic state, TRS will be preserved with the spin-up electrons (holes) occupying the conduction (valence) FB. Under an external bias, the dissociated spin-up electrons conduct via the chiral edge state within the topological gap between the conduction FB and the dispersive band above (see solid red line in figure 2(c)), and spin-up holes conduct via the chiral edge state within the topological gap between the valence FB and the dispersive band below (see dashed red line in figure 2(c)). The spin-up electron and the spin-up hole propagate in the same direction along the two opposite edges of a ribbon sample (see figure 2(c) lower panel), equivalent to the spin-up electron and the spin-down electron along the opposite direction, corresponding to two copies of QSHE. As a result, an EQSHE is featured with a spin Hall conductivity $\sigma_{xy}^s = 2 \cdot e/4\pi$, as shown in figure 2(c). Note that although the triplet exciton is dark, triplet excitonic state can be converted from singlet state through intersystem conversion [27, 28].

For both the singlet EQAHE and triplet EQSHE, a stringent condition of CPI between the two FBs can be realized by FBs-enabled EI state [12], as we show below. The highly localized wavefunction of yin-yang FBs renders a large e – h wavefunction overlap, which strongly enhances Coulomb’s interaction to reduce the screening. Consequently, the increased exciton binding energy exceeds the band gap, leading to an EI state. Also, the FBs enhance the exchange interaction that leads to a large singlet-triplet splitting, favoring the formation of triplet EI state. Importantly, different from conventional EI state with dispersive bands, the unique EI state with two FBs of vanishing band width allows for CPI.

Next, we discuss the creation of yin-yang FBs in a lattice model. It is well-known that a Kagome lattice hosts a FB [29–33], which lies either above or below two dispersive bands depending on the sign of lattice hopping [34, 35]. Thus, to have two FBs, a natural place to start with is to have two atoms on every Kagome lattice site, i.e. a diatomic (dumbbell) Kagome lattice, as shown in figure 3(a). A tight-binding Hamiltonian can be written as

$$H = t_1 \sum_{\langle ij \rangle \alpha} c_{i\alpha}^\dagger c_{j\alpha} + t_2 \sum_{\langle\langle ij \rangle\rangle \alpha} c_{i\alpha}^\dagger c_{j\alpha} + t_3 \sum_{\langle\langle\langle ij \rangle\rangle\rangle \alpha} c_{i\alpha}^\dagger c_{j\alpha} + i\lambda \sum_{\langle\langle ij \rangle\rangle \alpha\beta} \frac{2}{\sqrt{3}} (\hat{\mathbf{r}}_{ij}^1 \times \hat{\mathbf{r}}_{ij}^2) \cdot \sigma_{\alpha\beta}^z c_{i\alpha}^\dagger c_{j\beta}. \quad (1)$$

The first term represents the nearest-neighbor (NN) intra-dumbbell hopping, $c_{i\alpha}^\dagger$ ($c_{i\alpha}$) is the electron creation

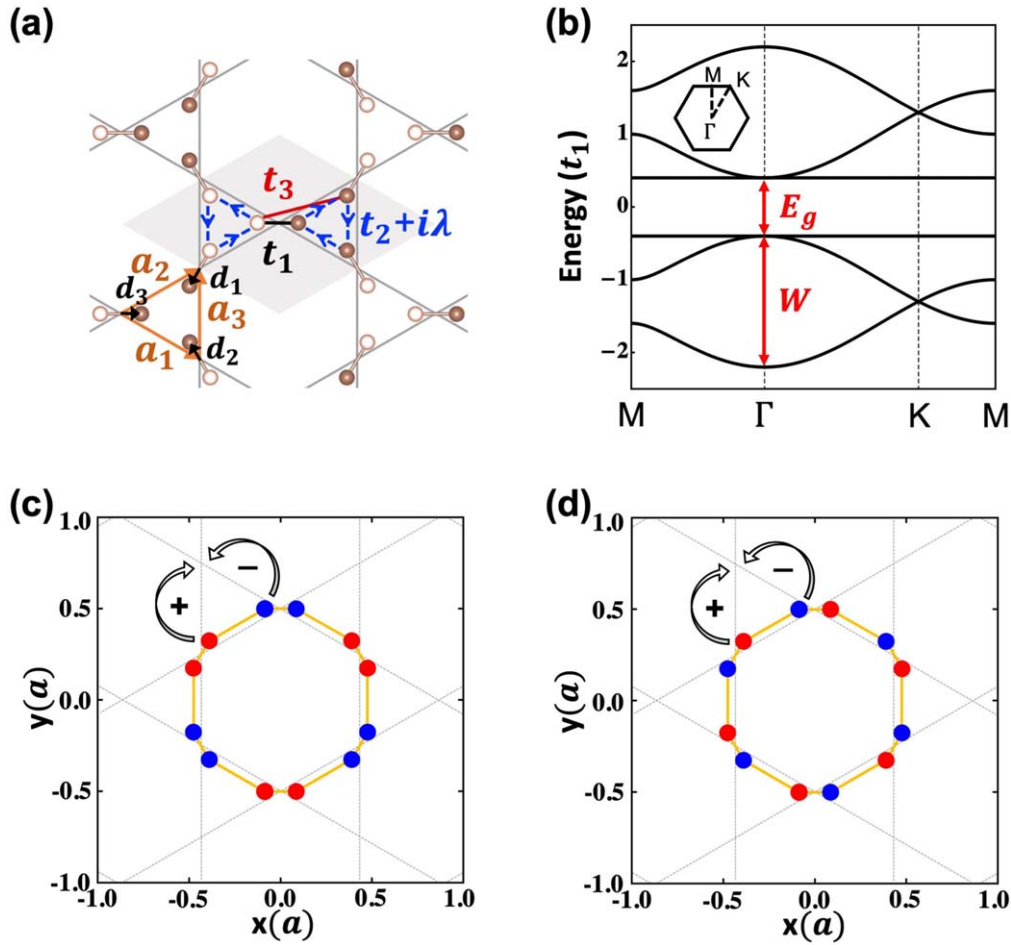


Figure 3. Creation of the yin-yang FBs in a diatomic Kagome lattice. (a) The diatomic Kagome lattice with a dumbbell (two atoms) on every Kagome lattice site. The shaded area indicates the unit cell. t_1 , t_2 , and t_3 represent the NN intra-dumbbell, 2NN inter-dumbbell and 3NN cross-dumbbell hopping, respectively. λ is the SOC strength. (b) The ideal band structure containing yin-yang FBs, obtained with $t_1, t_2 = 0$, $t_3 = 0.3t_1$ and $\lambda = 0$. The inset shows the first Brillouin zone. (c) Distribution of real-space wavefunction of the valence (yin) FB. Red and blue dots represent positive and negative phases of the wavefunction at the position, respectively. (d) Same as (c) for the conduction (yang) FB.

(annihilation) operator on site i of spin α . The second (third) term represents 2NN inter-dumbbell (3NN cross-dumbbell) hopping. The fourth term represents spin-orbit coupling (SOC) with a coupling strength λ , $\hat{r}_{ij}^{1,2}$ are the 2NN unit vectors; $2/\sqrt{3} |\hat{r}_{ij}^1 \times \hat{r}_{ij}^2| = \pm 1$ [8]. $\sigma_{\alpha\beta}^z$ is the Pauli matrix; α and β are spin indices.

Considering only the NN (t_1) and 2NN hopping (t_2), one would obtain a band structure consisting of either one set of Dirac bands plus another set of four bands, or two sets of Kagome bands but both having FB above (or below) the dispersive bands for $t_2 < t_1$. Interestingly, it is found that the trick to obtaining two sets of Kagome bands with opposite signs of hopping, i.e. the yin-yang FB (opposite Chern numbers), is to include a 3NN hopping (t_3) that adds a ‘cross-hopping’ between two sub-Kagome lattices. A phase diagram of band structures in the parameter space of hopping parameters has been shown before [25]. The condition for the existence of two yin-yang FBs is $0.5t_1 > t_3 > 0.5t_2$. Here, for simplicity, we neglect t_2 , which will not affect the band structure qualitatively. We note that the diatomic Kagome lattice model is related to the so-called hexagonal star lattice

[36–40], but people have viewed the same lattice as having a triangle atomic basis in a hexagonal lattice instead of a diatomic basis in a Kagome lattice without realizing yin-yang FBs and their intriguing topological properties.

An ideal yin-yang FB structure is shown in figure 3(b). The eigenvalues of the yin-yang FBs are $E_{Y^-, Y^+} = \pm(t_1 - 2t_3)$. To better understand the physical origin of FBs, their Bloch states are derived as $\Psi_{Y^-, Y^+}^\dagger(\mathbf{k}) = \sum_{i=1}^3 (-1)^i \text{sink}_i [\mp e^{-ik \cdot d_i} c_{k,i}^\dagger - e^{ik \cdot d_i} c_{k,i+3}^\dagger]$, where $k_n = \mathbf{k} \cdot \mathbf{a}_n$, \mathbf{a}_n is the lattice vector; d_n represents the vector pointing from the Kagome site to the dumbbell atom, as shown in figure 3(a). Fourier transforming the FB Bloch states into real space, one has

$$\Psi_{Y^-, Y^+}^\dagger(\mathbf{R}) = \frac{1}{\sqrt{12}} \times \left\{ \sum_{i=1}^6 \pm (\mp 1)^i c_i^\dagger + \sum_{i=7}^{12} (\mp 1)^i c_i^\dagger \right\}, \quad (2)$$

where i runs over the twelve vertices of a dodecahedron centered at a chosen position \mathbf{R} , as shown in figures 3(c) and (d). The phase distribution of the real-space wave functions of

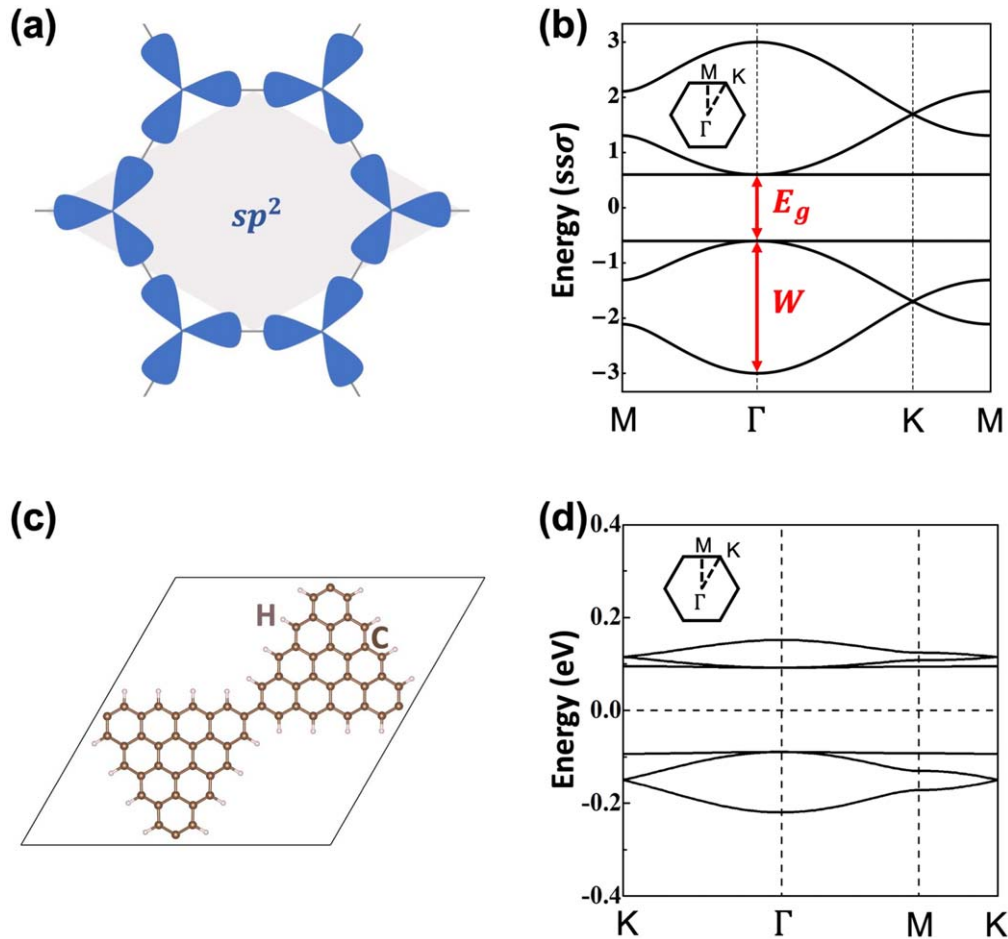


Figure 4. (a), (b) An sp^2 hexagonal lattice (left, the shaded area indicates the unit cell) exhibiting yin-yang FBs (right), calculated with $sp\sigma = -0.8ss\sigma$, $pp\sigma = -0.4ss\sigma$, $pp\pi = 0$. The band gap between the two FBs $E_g = 3pp\sigma$ and the band width $W = 3|ss\sigma - pp\sigma/2|$. The inset shows the first BZ. (c) Lattice structures for the superatomic graphene lattice with the size of 9×9 times of the original graphene unit cell. (d) Typical yin-yang FBs of (c) with the molecular sp^2 orbitals in a hexagonal lattice (similar to (a), (b)). The hopping appears to decay slowly due to the special lattice and orbital symmetry so as to meet the condition of $t_3 > 0.5t_2$ for realizing the yin-yang FBs in the dumbbell Kagome model.

both yin and yang FB display a perfect pattern of destructive interference (or phase cancellation), expected for a FB [41], so that lattice hopping out of the plaquette is prohibited (see arrows in figures 3(c) and (d)). Moreover, looking at the dumbbell on each Kagome lattice site, the valence (conduction) FB wave functions are of the same (opposite) phase, indicating a bonding (anti-bonding) state between the two sub-Kagome lattices. This is consistent with the negative versus positive lattice hopping for yin versus yang FB.

The SOC opens four topological gaps, two between FB and Dirac band and two at the Dirac points (figure S2(a)). The system would be a QSH insulator if the Fermi energy were in one of them, as illustrated by the calculated spin Hall conductivity [32] showing four quantized plateaus of $\sigma_{xy}^s = 2 \cdot e/4\pi$ within the SOC gaps (figure S3). However, of our interest here is the two isolated FBs that carry opposite Chern numbers in each spin channel, forming an enantiomorphic pair. The Berry curvatures for the two spin-up FBs (see figure S2(b)) look like a mirror image of each other having negative and positive values in the conduction and

valence FBs respectively. The spin-down FB Berry curvatures are just the opposite of figure S2(b). Integration of Berry curvatures gives the opposite Chern numbers for the two FBs which are optically active, whose single-particle photoexcitation properties has been discussed previously [25].

Now we discuss candidate material systems to illustrate the feasibility of realization of EQAHE and EQSHE, in association with the FB-EI state [12]. One system is the sp^2 basis in a hexagonal lattice (Figure 4(a)), which gives rise to yin-yang FBs (figure 4(b)). It can be realized in molecular lattices, such as a superatomic graphene lattice made of triangular graphene flakes (figure 4(c)). DFT calculated band structures are shown in figure 4(d) (see computational methods in supplementary material). For a small graphene flake (structural motif), the 5×5 superlattice shows the s -like molecular orbitals (figures S4(a), (b)) and 7×7 superlattice shows the (p_x, p_y) -like molecular orbitals (figures S4(c), (d)). With the increasing size of graphene flake (9×9 superlattice), the carbon p_z orbitals hybridize into molecular sp^2

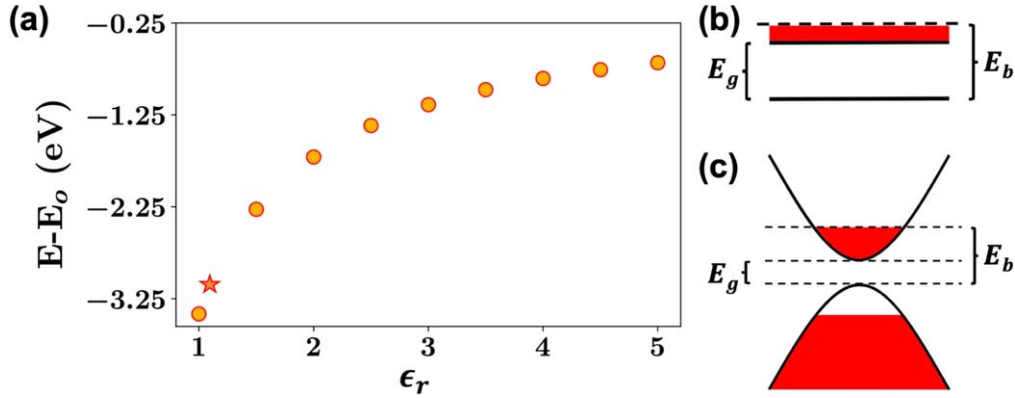


Figure 5. (a) Energy of the CPI-EI state (E) with respect to $|vac\rangle$ state (E_0) as a function of relative dielectric constant (ϵ_r). Star symbol indicates the values for superatomic graphene lattice. Negative values indicate spontaneous formation of CPI-EI state. (b), (c) schematic comparison between (b) CPI in FB-EI state and (c) excitonic instability in parabolic-band EI state without CPI. In (b), the band width of the conduction FB is zero, all the excitons have a binding energy (E_b) exceeding the band gap (E_g) to allow for CPI. Fermi levels are assumed to be in the gap.

orbitals on the hexagonal lattice, hosting the yin-yang FBs (figures 4(c), (d)).

Interestingly, our recent work shows the existence of a triplet EI state in the 9×9 superatomic graphene lattice due to the highly localized and overlapped electron and hole wave functions that are intrinsic to the two FBs, based on DFT-GW calculations [12]. In the EI state, the exciton binding energy exceeds the band gap; the electron-hole pairs become the *ground-state* quasiparticles to be more stable than separated electrons and holes and have an infinite lifetime, so that with continuous illumination, CPI between yin and yang FB is achievable. To confirm this, we have performed exact diagonalization calculations of a many-body lattice Hamiltonian with Coulomb interactions projected onto the two yin-yang FBs, to assess the stability of the EI state with CPI (N excitons in a lattice with N sites), beyond the formation of one exciton treated by the DFT-GW calculation [12]. A form of screened Coulombs potential $V(q) = e^2 / (4\pi\epsilon_0\epsilon_r S) \cdot 2\pi / \sqrt{q^2 + r_0^2}$ is adopted for electron-electron interaction [42], where e is the electron charge, ϵ_0 is the dielectric constant of vacuum, ϵ_r is the relative dielectric constant of the material over vacuum, S is the area of a unit cell, and r_0 measures the screening strength, which is set to $2/\{\text{lattice constant}\}$.

With SOC, gaps open to make both FBs isolated (figure S2(a)). Then, one can project the interaction onto two FBs and solve the problem in a Hilbert sub-space where the occupation of electrons will only vary between the two FBs all other bands will always remain filled or empty. This leads to a low-energy effective Hamiltonian,

$$\begin{aligned}
 H_{\text{eff}} = & \sum_{i,k} \epsilon_{i,k} c_{i,k}^\dagger c_{i,k} \\
 & + \sum_{i,j,i',j',\{k\}} \delta_{k_1+k_2-k_3-k_4}^{2\pi} \\
 & \times V(\{k\})_{i,j,i',j'} c_{i,k_1}^\dagger c_{j,k_2}^\dagger c_{i',k_3} c_{j',k_4}, \quad (3)
 \end{aligned}$$

where indices i, j, i', j' run over the two FBs, $\epsilon_{i,k}$ is the single-particle FB energy, and $V(\{k\})_{i,j,i',j'}$ contains the

single-particle FB wave functions and phase factors arising from the unitary transformation since single-particle Hamiltonian must be in the Bloch's form. The interaction part of H_{eff} contains 16 terms in the summation for all the conserved momenta set $\{k\}$. They include direct (exchange) $e-h$ interaction, $e-e$ ($h-h$) repulsion in the conduction (valence) FB, and other momentum conserving processes in which electrons are scattered between states of different occupation numbers. Since we are interested in the state with completely occupied or empty bands, we can ignore the non-occupation-conserving processes [43] and solve the Hamiltonian for complete excitation, i.e. the CPI state, using the first 6 terms only. The basis states are given by $\prod_{k'} c_{con,k'}^\dagger \prod_k c_{val,k} |vac\rangle$, and $|vac\rangle$ is defined as the fully occupied valence FB. More details of exact diagonalization calculations are available in supplementary material, section V.

We use a finite system with $N_x \times N_y$ unit cells (total states = $2 \times N_x \times N_y$). The excitation factor is $v_{ex} = N_e / (N_x \times N_y)$, where N_e is the number of electrons in the conduction FB. Under periodic boundary condition, we implement translational symmetries and diagonalize the Hamiltonian in each momentum sector $q = ((2\pi k_x)/L_x, (2\pi k_y)/L_y)$ with k_x and k_y being the integers. The single-particle energies and wave functions are calculated at $t_1 = 1; t_2 = 0; t_3 = 1/3$, and $\lambda = 0.05$. For CPI, $v_{ex} = 1$, and there is only one momentum sector since all the electrons are excited, i.e. all electron and hole states are fully occupied. Finally, we calculate the energy of this state with respect to that of $|vac\rangle$. Convergence test has been done with respect to system size (figure S6). In figure 5(a), we plot the energy of the CPI state as a function of ϵ_r . Negative values indicate spontaneous formation of CPI, i.e. the CPI-EI state, in all ranges of ϵ_r . This happens for a strong interaction regime when the $e-h$ attraction can overcome the $e-e$ and $h-h$ repulsion. This is consistent with our previous finding [12] that the FBs inherently reduce the screening, leading to a very low $\epsilon_r \sim 1$ (marked as star in figure 5(a)).

It is important to note that the CPI can only be achieved with the 'FBs-enabled' EI state but not the conventional EI

state with dispersive bands, as illustrated in figures 5(b), (c). This is because in order for the CPI to occur, not only the exciton binding energy has to exceed band gap as in any EI state, but also to exceed the gap by a value larger than the width of the CB, which can only be met by the FB-EI state (figure 5(b)) where all the excitons are stable. With dispersive parabolic bands, the high-energy excitons above the binding energy are unstable (figure 5(c)), then the resulting Hall conductivity will be non-quantized. Similarly, the EQAHE/EQSHE is fundamentally different the non-equilibrium valley Hall effect [15–19] with non-quantized charge/spin Hall conductivity without the formation of EI state.

The EQAHE/EQSHE may provide an effective means for experimental detection of the FB-EI state, which could be challenging otherwise as excitons are neutral quasiparticles. For reaching the CPI associated with EI state, low-temperature measurement is needed below the critical temperature for EI transition [44]. Also, as for observing the conventional QAHE and QSHE, the temperature needs to be lower than the topological gap. We envision the yin-yang FB structure can exhibit much rich and intriguing physics beyond single FB structure. Fundamentally, the yin-yang FBs may support fractional excitation, giant circular dichroism (CD) [25], anomalous excitonic behavior (e.g. Wigner crystallization of excitons [45, 46]), topological superconductivity [47–49], and a two-level model of quantum entanglement [50]. Practically, they may find applications in topological optoelectronic devices (e.g. CD spectrometer, photodetector and laser) and quantum information and quantum computation devices. The yin-yang FBs may be found in more materials (see supplementary material section IV) [25] and should also be makeable in artificial systems, such as cold-atom [51, 52], photonic [53], optical [54, 55], and phononic lattices [56] and topological circuit [57].





Acknowledgments

We thank Drs. Zheng Liu, Congjun Wu, Di Xiao, and Chao Zhang for helpful discussions. This work is supported by U.S. DOE-BES (Grant No. DE-FG02-04ER46148). YZ and GS contributed equally to this work.

Data availability statement

The data that support the findings of this study are available upon reasonable request from the authors.

ORCID iDs

Yinong Zhou  <https://orcid.org/0000-0002-4427-0032>
 Hang Liu  <https://orcid.org/0000-0001-6586-3040>
 Zhengfei Wang  <https://orcid.org/0000-0002-0788-9725>
 Feng Liu  <https://orcid.org/0000-0002-3701-8058>

References

- [1] Klitzing K v, Dorda G and Pepper M 1980 *Phys. Rev. Lett.* **45** 494
- [2] Thouless D J, Kohmoto M, Nightingale M P and den Nijs M 1982 *Phys. Rev. Lett.* **49** 405
- [3] Laughlin R B 1983 *Phys. Rev. Lett.* **50** 1395
- [4] Haldane F D M 1983 *Phys. Rev. Lett.* **50** 1153
- [5] Haldane F D M 1988 *Phys. Rev. Lett.* **61** 2015
- [6] Kane C L and Mele E J 2005 *Phys. Rev. Lett.* **95** 226801
- [7] Bernevig B A, Hughes T L and Zhang S C 2006 *Science* **314** 1757–61
- [8] Kane C L and Mele E J 2005 *Phys. Rev. Lett.* **95** 146802
- [9] Sheng D, Weng Z, Sheng L and Haldane F 2006 *Phys. Rev. Lett.* **97** 036808
- [10] Chang C Z et al 2013 *Science* **340** 167–70
- [11] König M, Wiedmann S, Brüne C, Roth A, Buhmann H, Molenkamp L W, Qi X L and Zhang S C 2007 *Science* **318** 766–70
- [12] Sethi G, Zhou Y, Zhu L, Yang L and Liu F 2021 *Phys. Rev. Lett.* **126** 196403
- [13] Kohn W 1967 *Phys. Rev. Lett.* **19** 439
- [14] Jérôme D, Rice T and Kohn W 1967 *Phys. Rev.* **158** 462
- [15] Rycerz A, Tworzydło J and Beenakker C 2007 *Nat. Phys.* **3** 172
- [16] Akhmerov A and Beenakker C 2007 *Phys. Rev. Lett.* **98** 157003
- [17] Xiao D, Yao W and Niu Q 2007 *Phys. Rev. Lett.* **99** 236809
- [18] Yao W, Xiao D and Niu Q 2008 *Phys. Rev. B* **77** 235406
- [19] Xiao D, Liu G B, Feng W, Xu X and Yao W 2012 *Phys. Rev. Lett.* **108** 196802
- [20] Blöchl P E 1994 *Phys. Rev. B* **50** 17953
- [21] Kresse G and Joubert D 1999 *Phys. Rev. B* **59** 1758
- [22] Perdew J P, Burke K and Ernzerhof M 1996 *Phys. Rev. Lett.* **77** 3865
- [23] Kresse G and Furthmüller J 1996 *Phys. Rev. B* **54** 11169
- [24] Hobbs D, Kresse G and Hafner J 2000 *Phys. Rev. B* **62** 11556
- [25] Zhou Y, Sethi G, Zhang C, Ni X and Liu F 2020 *Phys. Rev. B* **102** 125115
- [26] Kambe T et al 2013 π -Conjugated Nickel Bis(dithiolene) Complex Nanosheet *Journal of the American Chemical Society* **135** 2462–5
- [27] Kasha M 1950 *Discuss. Faraday Soc.* **9** 14–9
- [28] Palotás J, Negyedi M, Kollarics S, Bojtor A, Rohringer P, Pichler T and Simon F 2020 *ACS Nano* **14** 11254–61
- [29] Mielke A 1992 *J. Phys. A* **25** 4335
- [30] Tang E, Mei J W and Wen X G 2011 *Phys. Rev. Lett.* **106** 236802
- [31] Parameswaran S, Kimchi I, Turner A M, Stamper-Kurn D and Vishwanath A 2013 *Phys. Rev. Lett.* **110** 125301
- [32] Wang Z, Su N and Liu F 2013 *Nano Lett.* **13** 2842–5
- [33] Zong Y, Xia S, Tang L, Song D, Hu Y, Pei Y, Su J, Li Y and Chen Z 2016 *Opt. Express* **24** 8877–85
- [34] Ohgushi K, Murakami S and Nagaosa N 2000 *Phys. Rev. B* **62** R6065
- [35] Guo H M and Franz M 2009 *Phys. Rev. B* **80** 113102
- [36] Yao H and Kivelson S A 2007 *Phys. Rev. Lett.* **99** 247203
- [37] Rüegg A, Wen J and Fiete G A 2010 *Phys. Rev. B* **81** 205115
- [38] Wen J, Rüegg A, Wang C C J and Fiete G A 2010 *Phys. Rev. B* **82** 075125
- [39] Chen M and Wan S 2012 *J. Phys. Condens. Matter* **24** 325502
- [40] Chen W C, Liu R, Wang Y F and Gong C D 2012 *Phys. Rev. B* **86** 085311
- [41] Zheng L, Feng L and Yong-Shi W 2014 *Chin. Phys. B* **23** 077308

- [42] Liu Z, Abouelkomsan A and Bergholtz E J 2021 *Phys. Rev. Lett.* **126** 026801
- [43] Potasz P, Xie M and MacDonald A H 2021 *Phys. Rev. Lett.* **127** 147203
- [44] Du L, Li X, Lou W, Sullivan G, Chang K, Kono J and Du R R 2017 *Nat. Commun.* **8** 1–8
- [45] Wu C, Bergman D, Balents L and Sarma S D 2007 *Phys. Rev. Lett.* **99** 070401
- [46] Wu C and Sarma S D 2008 *Phys. Rev. B* **77** 235107
- [47] Miyahara S, Kusuta S and Furukawa N 2007 *Physica C* **460** 1145–6
- [48] Kobayashi K, Okumura M, Yamada S, Machida M and Aoki H 2016 *Phys. Rev. B* **94** 214501
- [49] Cao Y, Fatemi V, Fang S, Watanabe K, Taniguchi T, Kaxiras E and Jarillo-Herrero P 2018 *Nature* **556** 43
- [50] Horodecki R, Horodecki P, Horodecki M and Horodecki K 2009 *Rev. Mod. Phys.* **81** 865
- [51] Ruostekoski J 2009 *Phys. Rev. Lett.* **103** 080406
- [52] Jo G B, Guzman J, Thomas C K, Hosur P, Vishwanath A and Stamper-Kurn D M 2012 *Phys. Rev. Lett.* **108** 045305
- [53] Russell P S J, Hölzer P, Chang W, Abdolvand A and Travers J 2014 *Nat. Photon.* **8** 278
- [54] Zhang S, Kang M, Huang H, Jiang W, Ni X, Kang L, Zhang S, Xu H, Liu Z and Liu F 2019 *Phys. Rev. B* **99** 100404
- [55] Jiang W, Kang M, Huang H, Xu H, Low T and Liu F 2019 *Phys. Rev. B* **99** 125131
- [56] Xue H, Yang Y, Gao F, Chong Y and Zhang B 2019 *Nat. Mater.* **18** 108
- [57] Koch J, Houck A A, Le Hur K and Girvin S 2010 *Phys. Rev. A* **82** 043811